Article

Photoactivatable RNA Tags for Subcellular Photolabeling of RNA

Zhenyin Chen,[♦] Haodong Jiang,[♦] Lin Yuan, Tuoxin Yao, Xiaoxiao Rong, Wankai Gao, Chenhang Zeng, Liuqin He, Yulong Yin, Samie R. Jaffrey, Fangqing Zhao, Jinyang Zhang,* Pingyong Xu,* and Xing Li*
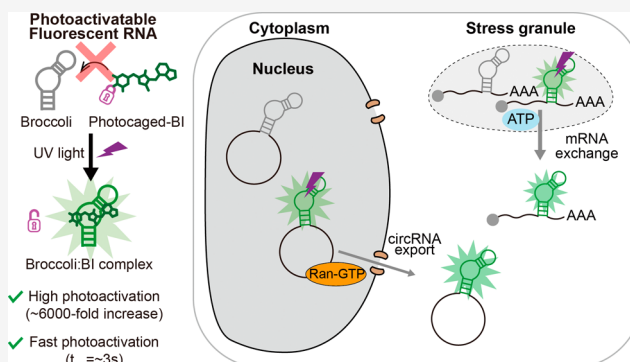
ACCESS | 📊 Metrics & More | 📖 Article Recommendations | 🆘 Supporting Information

ABSTRACT: Photoactivatable fluorescent proteins enable precise analysis of subcellular protein dynamics, but a comparable approach for photoactivated tagging subcellular RNA remains lacking. Here, we develop PA-Broccoli, a photoactivatable fluorescent RNA tag that mimics photoactivatable green fluorescent proteins (PA-GFP). Similar to PA-GFP, PA-Broccoli is initially nonfluorescent but emits intense green fluorescence after ultraviolet light irradiation. Notably, complete photoactivation of PA-Broccoli results in a 6000-fold fluorescence enhancement with a rapid activation ($t_{1/2} = \sim 3$ s), outperforming PA-GFP in sensitivity and speed by 1–2 orders of magnitude. Using PA-Broccoli, we first uncovered that cytoplasmic RNAs display restricted mobility compared to proteins. In addition, we revealed that circular RNAs undergo Ran-GTP-dependent nuclear export and slower cytoplasmic accumulation than linear mRNAs. Third, real-time imaging of mRNA within stress granules indicates that mRNA exchange throughout these granules is energy-dependent. These findings establish PA-Broccoli as a transformative tool for live-cell RNA tracking, offering unprecedented insights into RNA dynamics and regulatory mechanisms.

■ INTRODUCTION

Genetically encoded fluorescent tags combined with advanced optical imaging have emerged as powerful tools for spatiotemporal monitoring of cellular biomolecules. Notably, fluorescent protein-based tags have been widely used for protein imaging since the discovery of green fluorescent protein (GFP).[1] However, traditional fluorescent protein tags suffer from continuous fluorescence, which is a significant limitation for tracking proteins in specific subcellular compartments. This fundamental limitation spurred the development of photoactivatable fluorescent proteins that can be selectively "switched on" by light irradiation.[2] Among these, photoactivatable GFP (PA-GFP) enables precise spatiotemporal labeling of protein subpopulations, revolutionizing studies of protein trafficking and organelle interactions[2–10]

Like proteins, RNA plays crucial roles in cellular processes. This has motivated the development of fluorescent RNA tags for RNA imaging in live cells. Fluorescent RNAs are RNA sequences that bind and activate otherwise nonfluorescent small molecule fluorophores. By fusing an RNA with a fluorescent RNA, fluorescence can be genetically encoded into the RNA. To date, fluorescent RNAs have been used for elucidating RNA function, including monitoring noncoding RNA transcription rates, imaging single RNA or RNA aggregates, and tracking RNA-protein interactions.[11–14] While fluorescent RNAs have advanced live-cell RNA imaging, they share the same limitation of constitutive fluorescent protein tags. The development of photoactivatable RNA tags would fill a critical gap in studying subcellular RNA localization, transport, and other dynamic processes. However, such photoactivatable RNA tools for subcellular RNA imaging remain undeveloped, creating a critical technological gap in RNA biology research.

To address this critical need, we present a photoactivatable fluorescent RNA tag designed for subcellular RNA imaging. Here, we used Broccoli as fluorescent RNA tags, an RNA sequence that binds and activates GFP-like fluorophores.[11,15,16] Therefore, Broccoli is an RNA mimic of GFP. By designing and optimizing a photocaged group on the GFP-like fluorophore, we constructed a photoactivatable Broccoli (PA-Broccoli) RNA tag. Similar to PA-GFP, PA-Broccoli exhibits minimal fluorescence until activated by UV irradiation, resulting in high fluorescence levels. Remarkably, PA-Broccoli outperforms PA-GFP with substantially higher photoactivation (~6000-fold versus ~15-fold photoactivation) and faster activation kinetics ($t_{1/2}$ of ~3 s versus ~50 s). Thus, PA-Broccoli mimics the optical behavior of PA-GFP with improved sensitivity and kinetics.

A

Table 1. Photophysical and Binding Properties of Different FLAPs *in Vitro*

	excitation (nm)	emission (nm)	preactivation			postactivation			photoactivation fold
			extinction coefficient (ε) [$M^{-1} \cdot cm^{-1}$]	quantum yield (φ)	brightness[a]	ε [$M^{-1} \cdot cm^{-1}$]	φ	brightness	
Rhodamine 6G	525	547	116,000	0.95	100				
BI	425	500	42,500	0.0004	0.02				
Broccoli:BI[15]	470	505	33,600	0.88	29.78				
PA3-BI	470	505	23,100	0.00017	0.004	42,500	0.0004	0.02	4.3-fold
Broccoli:PA3-BI (PA-Broccoli)	470	505	23,750	0.0002	0.005	33,600	0.88	29.78	6224-fold
PA-GFP	475	517	14,280	0.09	1.29	23,260	0.76	17.8	13.8-fold

[a]The brightness (extinction coefficient × quantum yield) of each fluorophore or complex is relative to Rhodamine 6G.
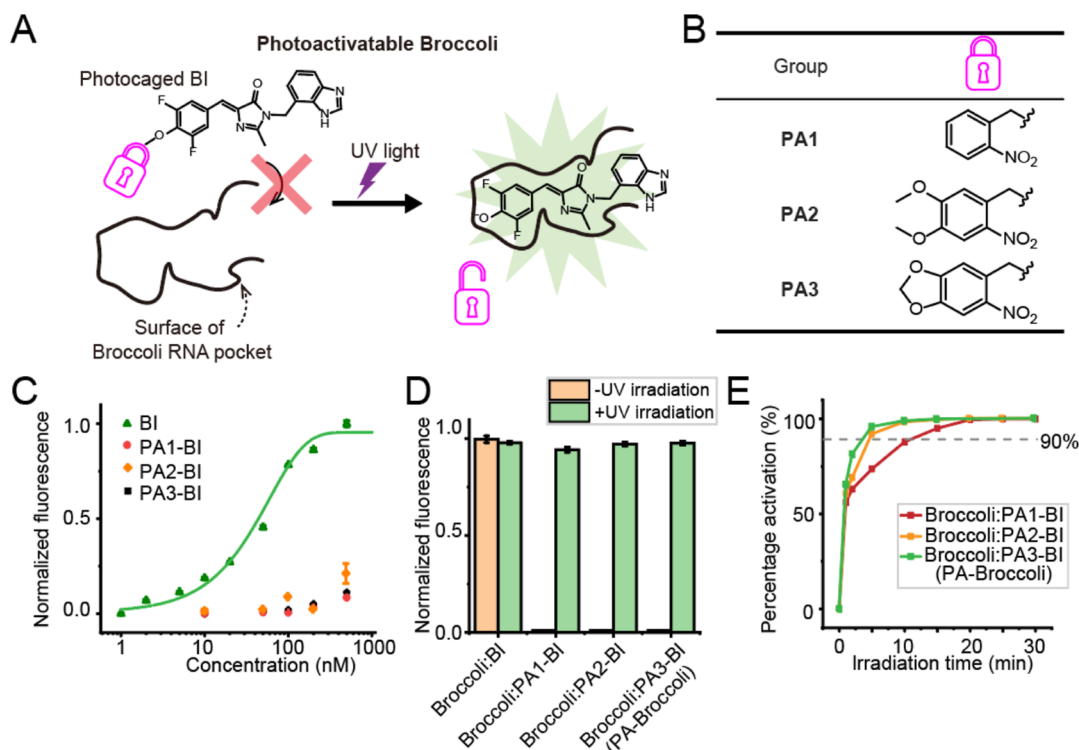

Figure 1. Development of a photoactivatable fluorescent RNA tag with Broccoli. (A) Design principle of photoactivatable Broccoli RNA tag. A bulky photoactivatable substituent (magenta lock) conjugated to the hydroxyl group of BI sterically blocks fluorophore binding to the Broccoli aptamer, resulting in little fluorescence. Upon UV irradiation (purple lightening), the photoactivatable substituent detaches, allowing BI to bind and activate Broccoli fluorescence. (B) Chemical structure of photoactivatable BI derivatives. BI was modified with three different photoactivatable groups—*ortho*-nitrobenzyl (PA1),[23] 4,5-methylenedioxy-2-nitrobenzyl (PA2),[24] and 3,4-(methylenedioxy)-6-nitrophenylethoxycarbonyl (PA3)[25] groups, respectively. (C) Broccoli binds BI rather than PA-BIs before photoactivation. Fluorescence titration assays (50 nM Broccoli, 1−500 nM fluorophores) revealed Broccoli selectively binds unmodified BI (Ex = 470 nm, Em = 505 nm). Photoactivatable variants (PA1-BI, PA2-BI, PA3-BI) showed no binding, confirming the caging groups block aptamer recognition. Data represent mean values ± s.d. for n = 3 independent experiments. (D) *In vitro* photoactivation of Broccoli:PA-BIs. PA1-, PA2- and PA3-BI (1 μM) were incubated with Broccoli (10 μM) and irradiated using a UV lamp (7 mW/cm^2) for 30 min. Then, Broccoli fluorescence (Ex = 470 nm, Em = 505 nm) was measured with a spectrometer. Before UV irradiation, all Broccoli:PA-BIs showed minimal fluorescence. After 30 min of irradiation, PA1-, PA2- and PA3-BI showed completed fluorescence activation in the presence of Broccoli, reaching the overall fluorescence to that of Broccoli:BI. Data represent mean values ± s.d. for n = 3 independent experiments. (E) Broccoli:PA3-BI (PA-Broccoli) exhibits a fast photoactivation rate. UV irradiation (7 mW/cm^2) of Broccoli:PA-BI complexes (1 μM:10 μM) showed PA3-BI achieved 90% activation in 3 min, compared to 5 min (PA2-BI) and 10 min (PA1-BI). PA3-BI was therefore designated PA-Broccoli. Data represent mean values ± s.d. for n = 3 independent experiments.

The high fluorescence sensitivity and fast activation kinetics of PA-Broccoli enabled precise spatiotemporal photolabeling of subcellular RNA. To explore the application of PA-Broccoli tags, we dynamically tracked the nuclear export of circular RNAs and linear mRNAs, and found that circular RNAs are exported from the nucleus via a Ran-GTP-dependent pathway and accumulate slowly in the cytoplasm compared to linear mRNAs. Moreover, we used PA-Broccoli to spatiotemporally track mRNA dynamics within stress granules, revealing the ATP dependency of mRNA export. These findings highlight the photoactivatable fluorescent RNA tag as a valuable tool for spatiotemporal RNA imaging in living cells.

■ RESULTS

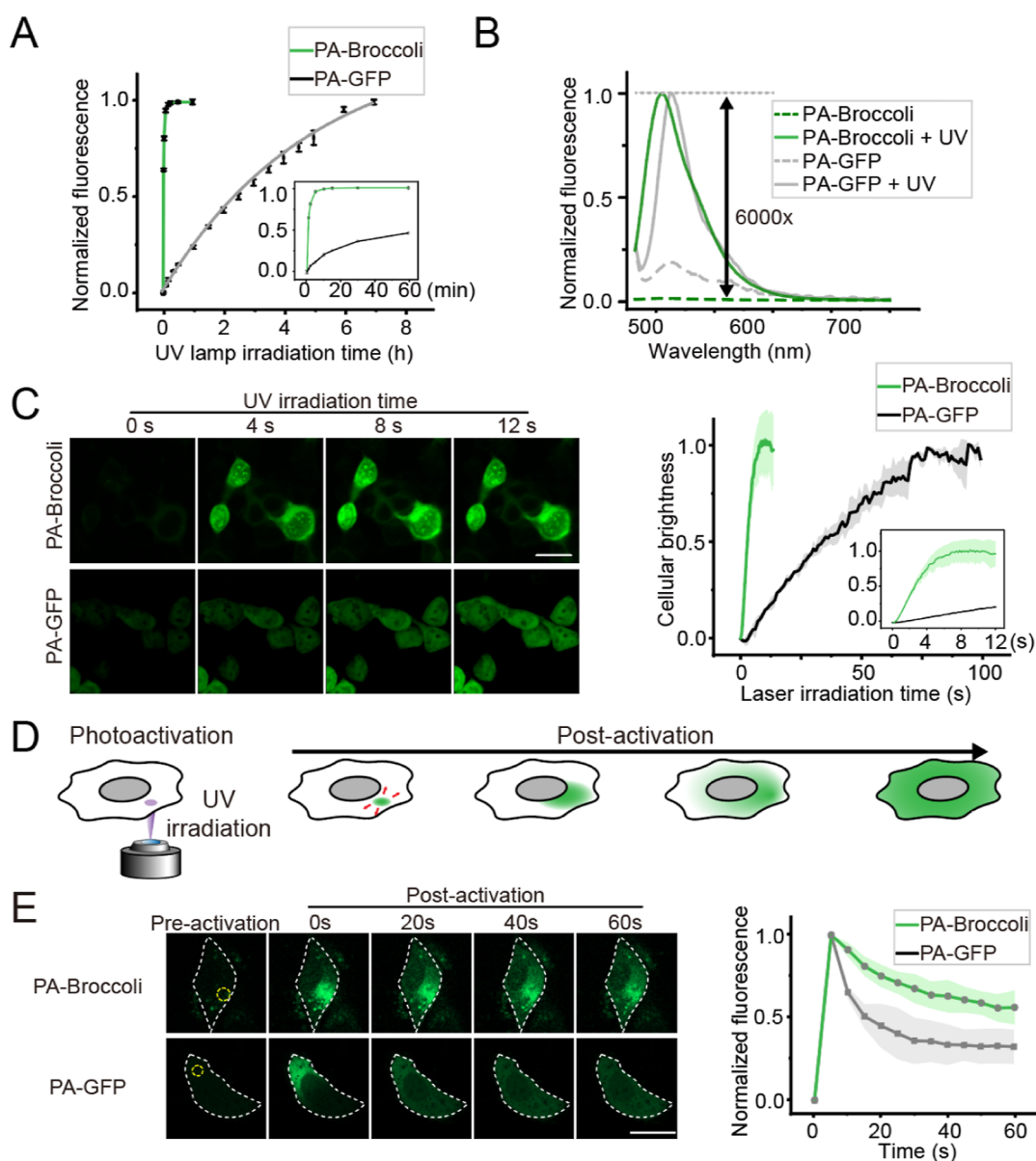### Generation and Optimization of a Photoactivatable Fluorescent RNA Tag PA-Broccoli. To develop photo-

Figure 2. PA-Broccoli shows significantly higher and faster photoactivation compared to PA-GFP. (A) PA-Broccoli exhibits a faster activation rate compared with PA-GFP. We photoactivated PA-Broccoli and PA-GFP for different time points and measured their fluorescence (PA-Broccoli: Ex = 470 nm, Em = 505 nm. PA-GFP: Ex = 475 nm, Em = 517 nm. UV irradiation power: 7 mW/cm^2). PA-Broccoli reached saturation in 5 min versus 7 h for PA-GFP. Data represent mean values ± s.d. for n = 3 independent experiments. (B) PA-Broccoli shows markedly higher fluorescent enhancement than PA-GFP upon photoactivation. To determine the fluorescent enhancement after irradiation, both PA-Broccoli (1 μM) and PA-GFP (1 μM) were irradiated with a UV lamp (7 mW/cm^2) until fully photoactivated. PA-Broccoli exhibited a ~6000-fold increase in peak emission fluorescence, a stark contrast to the ~13-fold enhancement observed with PA-GFP after photoactivation. (C) PA-Broccoli is rapidly photoactivated compared to PA-GFP in living cells. To photoactivate PA-Broccoli in living cells, we incubated Broccoli-expressing HEK293T cells with PA3-BI (10 μM) and continuously irradiated with a 405 nm laser (0.2 W/cm^2). As a control, cells expressing PA-GFP were subjected to the same laser conditions. PA-Broccoli and PA-GFP fluorescence were imaged with 488 nm laser excitation (0.25 W/cm^2), and a bandpass emission filter that transmits 525 ± 25 nm light. PA-Broccoli exhibited rapid fluorescence activation during the irradiation, with a $t_{1/2}$ of ~3 s. In contrast, PA-GFP fluorescence exhibits a $t_{1/2}$ of ~40 s of irradiation. We then calculated the photoactivation rate as the initial fluorescence increase per unit time (slope), which was ~17.2 for PA-Broccoli compared to 0.017 for PA-GFP, indicating that PA-Broccoli activates approximately 1000 times faster than PA-GFP in living cells. Scale bar, 20 μm. The fluorescence activation curve was collected from n = 10 cells from three independent experiments. (D) Schematic representation of local irradiation of a subcellular region of interest (ROI) in a single cell. Using laser scanning confocal microscopy, a defined ROI (purple circle) was able to be irradiated within a single live cell to locally photoactivate PA-Broccoli (green circle). (E) Cellular RNA fused with PA-Broccoli diffused rapidly compared to cellular protein fused with PA-GFP tag. We locally irradiated a 2 μm diameter ROI (yellow circle) in Broccoli-expressing HEK293T cells with a 405 nm laser (5 W/cm^2) and subsequently imaged the entire cell. As a control, we locally photoactivated PA-GFP in HEK293T cells under the same conditions. Both PA-Broccoli- and PA-GFP-expressing cells exhibited immediate fluorescence enhancement in the irradiated area. PA-GFP fluorescence in the ROI reached a plateau after ~40 s, slightly above the initial value, with a $t_{1/2}$ of ~13 s. In contrast, the fluorescence of locally activated PA-Broccoli RNA remained, showing minimal diffusion even after 60 s. These results suggest that RNA dynamics are more constrained compared to protein diffusion in the cytoplasm. Both PA-Broccoli and PA-GFP fluorescence were imaged with 488 nm laser excitation, and a bandpass emission filter that transmits 525 ± 25 nm light. Data represent n = 10 cells from three independent experiments. Scale bar, 20 μm.

activatable RNA imaging tools, we used Broccoli as the fluorescent RNA reporter.[11,15,16] Broccoli is an RNA sequence that can bind and activate the fluorescence of otherwise nonfluorescent DFHBI (3,5-difluoro-4-hydroxybenzylidene imidazolinone), a small molecule fluorophore mimic of GFP. In addition to DFHBI, several other GFP-like fluorophores, including DFHBI-1T(3,5-difluoro-4-hydroxybenzylidene imidazolinone-1-trifluoromethyl),[17] BI (3,5-difluoro-4-hydroxybenzylidene imidazolinone-1-benzoimidazole)[15] and TBI(3,5-difluoro-4-hydroxybenzylidene-2-thioxoimidazolidin-1-benzoimidazole)[18] also bind and light up Broccoli *in vitro* and in cells. Among these fluorophores, BI induced significantly high cellular Broccoli fluorescence (Ex = 470 nm, Em = 505 nm, φ = 0.88, ε = 33,600 M^{-1}·cm^{-1}, Table 1).[15] In addition, BI fluorophores show low cellular background at 10 μM (φ = 0.0004, ε = 42,500 M^{-1}·cm^{-1}, Table 1).[15] This is likely due to its minimal nonspecific binding to cellular components[19] and free intramolecular rotation in the unbound state. Once the intramolecular rotation is restricted by binding to Broccoli or in viscous environments like a high fraction of glycerol, BI fluorescence is markedly increased (Table 1, Figure S1).[20] Thus, BI exhibits aggregation-induced emission (AIE)-like features.[21] Consequently, we chose the Broccoli:BI system to design a photoactivatable RNA tag.

We next sought to convert Broccoli:BI into a photoactivatable fluorescent RNA tag. According to Broccoli/Spinach RNA crystal structure,[15,22] the hydroxyl group in BI faces a confined space within the Broccoli fluorophore-binding pocket. Thus, we hypothesized that introducing a bulky photoactivatable group to the hydroxyl of BI would prevent its binding to Broccoli (Figure 1A).[22] Therefore, the photocaged BI could not pair with Broccoli to produce RNA fluorescence. However, upon photoactivation, the photocaged BI could release the bulky photoactivatable group, allowing it to bind and activate Broccoli fluorescence (Figure 1A).

To explore this concept, we caged the hydroxyl group of BI with three different photoactivatable moieties: *ortho*-nitrobenzyl (PA1),[23] 4,5-methylenedioxy-2-nitrobenzyl (PA2),[24] 3,4-(methylenedioxy)-6-nitrophenylethoxycarbonyl (PA3),[25] respectively (Figure 1B). We synthesized PA1-BI by attaching an *ortho*-nitrobenzyl group (PA1)[24,25] to BI. This group is released under UV irradiation, allowing photoactivation. Considering that adding an electron-donating moiety to PA1 group may accelerate photoactivation rates,[26] we next synthesized PA2-BI (with a 4,5-methylenedioxy group in PA1) and PA3-BI (with a methylenedioxy group in PA1).[24,25] These PA-BIs could be photoactivated by UV irradiation and then bind Broccoli to emit fluorescence.

We next asked if these PA-BIs were unable to bind Broccoli before photoactivation. We measured the fluorescence intensity and binding affinity for Broccoli:PA-BIs and Broccoli:BI. We first incubated PA1-, PA2-, PA3-BI or BI (1 μM) with Broccoli RNA (10 μM) and measured the fluorescence with 470 nm excitation wavelength, which is the maximum excitation wavelength of Broccoli:BI.[15] Compared to highly fluorescent Broccoli:BI (φ = 0.88, ε = 33,600 M^{-1}·cm^{-1}, Table 1), all three Broccoli:PA-BIs exhibited minimal fluorescence (φ = 0.0002, ε = 23,750 M^{-1}·cm^{-1}, Table 1) before photoactivation. Moreover, we determined the dissociation constant (K_D) of Broccoli:PA-BIs and Broccoli:BI by measuring the fluorescence of Broccoli (50 nM) with various concentrations of PA-BIs or BI (0−500 nM). PA1-, PA2-, and PA3-BI all exhibit >1000-fold lower binding affinity (K_D > 10

μM) for Broccoli than BI (K_D = 56 nM) (Figure 1C). These results suggest that PA-BIs cannot be complexed with Broccoli and fluorescent prior to photoactivation.

We next photoactivated Broccoli:PA-BIs in vitro. To do this, we irradiated Broccoli:PA-BIs with UV light (365 nm) for 30 min and measured Broccoli fluorescence. Under these irradiation conditions, the photoactivatable moieties on PA-BIs are expected to be fully photoactivated,[23−25] allowing nearly complete conversion of PA-BIs to BI. As anticipated, all Broccoli:PA-BIs displayed extremely low fluorescence before irradiation (φ = 0.0002, ε = 23,750 M^{-1}·cm^{-1}, Table 1), even lower than free BI (φ = 0.0004, ε = 42,500 M^{-1}·cm^{-1}, Table 1). This is likely due to the nitrobenzyl group hindering electron donation, causing little background.[11,15,17,27] After 30 min of UV irradiation, these Broccoli:PA-BIs reached a similar overall fluorescence (φ = 0.88) comparable to Broccoli:BI (Table 1). Notably, all three Broccoli:PA-BIs exhibited ~6000-fold fluorescence activation at 505 nm peak emission postirradiation (Figure 1C,D). These data suggest that Broccoli:PA-BIs have an exceptionally low background, but can be completely photoactivated to produce equivalent brightness to Broccoli:BI, making it the highest-contrast photoactivatable fluorescent tag described to date.

To optimize Broccoli-based photoactivatable fluorescent RNA tags, we evaluated the photoactivation rates of three Broccoli:PA-BIs. We irradiated PA1-, PA2- and PA3-BI (1 μM) with Broccoli (10 μM) and measured the fluorescence at various intervals. Among these three pairs, Broccoli:PA3-BI exhibited the fastest photoactivation rate, reaching approximately 90% fluorescence within 3 min (Figure 1E). In contrast, Broccoli:PA2-BI and Broccoli:PA1-BI required 5 and 10 min, respectively, to achieve the same level of activation (Figure 1E). In addition, high-performance liquid chromatography−mass spectrometry (HPLC-MS) analysis confirmed that PA3-BI lost the PA-group and formed BI most rapidly (Figure S2). Therefore, we used Broccoli:PA3-BI system for subsequent experiments and termed the system PA-Broccoli.

PA-Broccoli Exhibits Outstandingly High and Fast Photoactivation Compared to PA-GFP. PA-Broccoli is derived from Broccoli which resembles GFP, and shows photoactivation properties similar to PA-GFP, therefore PA-Broccoli is the RNA mimic of PA-GFP. We then compared the photoactivation ability of PA-Broccoli with PA-GFP, a commonly used genetically encoded photoactivatable fluorescent tag.[2] PA-GFP can be activated from a nonfluorescent to a fluorescent state using UV irradiation, allowing selected subpopulations of the PA-GFP-fusion protein to be labeled and their movement tracked in living cells.[3]

To compare PA-Broccoli with PA-GFP, we irradiated the purified PA-GFP protein and PA-Broccoli under the identical UV light source and recorded the fluorescence at different time points. Prior to irradiation, both photoactivated tags exhibited low fluorescence (Figure 2A). However, PA-Broccoli demonstrated a rapid fluorescence increase, achieving 90% activation within 3 min, while PA-GFP required approximately 7 h to reach the same level (Figure 2A). Notably, the ~6000-fold fluorescence activation of Broccoli:PA-BIs is markedly higher than the ~13-fold activation observed with PA-GFP (Figure 2B).[2] These findings indicate that PA-Broccoli can be rapidly photoactivated with a far greater fold increase in fluorescence compared to PA-GFP.

We next asked whether PA-Broccoli fluorescence can be photoactivated in living cells. To do this, we expressed Broccoli

RNA in HEK293T cells using the Tornado-expressing system.[28] Then, we incubated the Broccoli-expressing cells with PA3-BI (10 μM) to form PA-Broccoli, and irradiated the cells with a UV laser (0.2 W/cm^2). As a control we expressed PA-GFP in cells in identical conditions. We observed an immediate increase in Broccoli fluorescence after the initial irradiation and the fluorescence reached 50% of its maximum value within ∼3 s (Figure 2C). In contrast, PA-GFP displayed a much slower activation rate, reaching 50% fluorescence after ∼40 s of irradiation (Figure 2C). Notably, the UV irradiation caused no detectable phototoxicity within 60 s exposure (Figure S3). In addition, PA-Broccoli can also be efficiently photoactivated in BL21 *Escherichia coli* (*E. coli*) cells with UV irradiation (Figure S3). These results confirm that PA-Broccoli can be efficiently photoactivated in living human and bacterial cells.

We next evaluated the photostability of PA-Broccoli. To do this, we continuously imaged cells expressing either PA-Broccoli or PA-GFP for 5 min under 488 nm laser excitation after UV photoactivation. PA-Broccoli retained ∼60% of its initial fluorescence, while PA-GFP retained only ∼40% after continuous excitation (Figure S5). This improved photostability of PA-Broccoli over PA-GFP is due to different photophysical mechanisms. After UV photoactivation, PA-BI fluorophores in PA-Broccoli can be converted into BI, which binds and lights up Broccoli through noncovalent interactions.[15] When a BI molecule is photobleached by 488 nm excitation, it can dissociate from Broccoli and be replaced by free BI in the cytoplasm. This dynamic exchange mechanism contributes to the high photostability of PA-Broccoli. In contrast, PA-GFP relies on an irreversibly bleachable internal chromophore that cannot be replenished, leading to faster fluorescence decay photobleaching.[29] Thus, the replaceable nature of BI in PA-Broccoli contributes to its improved performance over PA-GFP under prolonged illumination.

We next asked if this photoactivate strategy could be applied to other fluorogenic RNA:fluorophore systems in addition to Broccoli. To do this, we developed a PA-RhoBAST system, where RhoBAST binds and activates the small fluorophore tetramethylrhodamine-dinitroaniline (TMR-DN), a fluorophore-quencher conjugate.[30−32] By incorporating the PA3 group into TMR-DN, we assessed its fluorescence activation upon UV irradiation (Figure S6A,B). PA-RhoBAST exhibited low fluorescence prior toirradiation, and modest ∼15-fold fluorescence enhancement after photoactivation (Figure S6C), indicating a slower activation rate compared to PA-Broccoli (Figure S6D,E). This slower rate is likely due to the inductive effect of the carboxyl group on the TMR-DN, leading to slow dissociation of the photocaged group.[26] These results suggest that the PA group-caging strategy is broadly applied to construct diverse photoactivatable fluorescent RNA tags, with PA-Broccoli optimized as the highly sensitive photoactivatable tag.

We next sought to construct near-infrared (NIR)-activated PA-Broccoli to reduce phototoxicity during cell imaging. To do this, we installed the NIR-activated Cy-NN (cyanine dye IR-793 with *N,N′*-dimethylethylenediamine) group in BI to generate NIR-activated PA-Broccoli (Figure S7A).[33] When irradiated with a 680 nm NIR lamp (7 mW/cm^2), the NIR-activated PA-Broccoli showed significant fluorescence enhancement after 180 min (Figure S7B,C). In Broccoli-expressing cells treated with 10 μM of Cy-NN-BI, we observed noticeable fluorescence enhancement following 300 s of 685

nm laser irradiation, with minimal changes in cell morphology (Figure S7D,E). Compared with UV-activated PA-Broccoli, NIR-activated PA-Broccoli exhibited a slower activation rate both *in vitro* and in cells. These results suggest that we can construct NIR-activated PA-Broccoli by altering the photocaging moiety, though with slower activation kinetics compared to UV-activated PA-Broccoli.

Subcellular Photolabeling of RNA Using PA-Broccoli in Live Cells. We next photoactivated Broccoli-expressing cells in a region of interest (ROI). Previously reported photoactivatable fluorescent tags were used for tracking specific cell types in multicellular tissues by irradiating the indicated cell populations.[6] Therefore, we hypothesized that PA-Broccoli could similarly be utilized to label designated cell populations. To do this, we defined an ROI in a field of view and irradiated PA-Broccoli-expressing HEK293T cells within this region using a UV laser (5 W/cm^2) (Figure S8A). After irradiation, we observed increased fluorescence specificity in the ROI or defined patterns (Figure S8B,C). The fluorescence remained spatially confined within the ROI for at least 15 min, exhibiting minimal observable diffusion (Figure S8B,D). To further test whether photoactivated PA3-BI diffuses between cells, we photoactivated one of two adjacent Broccoli-expressing HEK293T cells. A strong fluorescence increase was detected in the photoactivated cell, whereas the neighboring cell showed only minimal fluorescence change over 15 min (Figure S9). Together, these results illustrate our ability to photolabel and track subpopulations of cells using PA-Broccoli.

We next asked if we could precisely photoactivate PA-Broccoli fusion RNA in a subcellular region to track RNA diffusion and migration in living cells. To accomplish this, we used scanning laser confocal microscopy to achieve pixel-wise illumination of localized subcellular ROIs (Figure 2D). We irradiated a locally defined spot in the cytoplasm of Broccoli-expressing cells with a focused 405 nm laser beam (5 W/cm^2) for 200 ms before imaging the entire cell. Right after photoactivation, we immediately observed the fluorescent locus (Figure 2E). We then recorded the fluorescence of the irradiated area, and compared it with the locally activated PA-GFP. Interestingly, while PA-GFP quickly diffused throughout the cytoplasm shortly after activation, PA-Broccoli exhibited a slower diffusion rate (Figure 2E). These observations suggest that cellular RNA likely exhibits slower molecular dynamics compared to proteins in the cytoplasm. This result is in agreement with the previous reports,[34−37] highlighting RNA propensity to interact with various proteins.[34,36,37]

To further confirm that the fluorescence diffusion is caused by Broccoli-fused RNA movement rather than fluorophore diffusion, we compared PA-Broccoli fluorescence spread in fixed and live cells. We expressed Broccoli in HEK293T cells and fixed the cells with polyoxymethylene. Then, we incubated the cells with PA3-BI and photoactivated a small region in the cytoplasm, and monitored fluorescence across the whole cell. In fixed cells, the Broccoli signal remained tightly localized throughout the 10 min imaging period, indicating that most photoactivated fluorophores diffuse slowly in 10 min within the irradiated subcellular region. In contrast, live cells showed rapid fluorescence spreading throughout the cytoplasm within 3 min (Figure S10). These results suggest that the fluorescence spreading was primarily driven by RNA movement, rather than fluorophore diffusion.
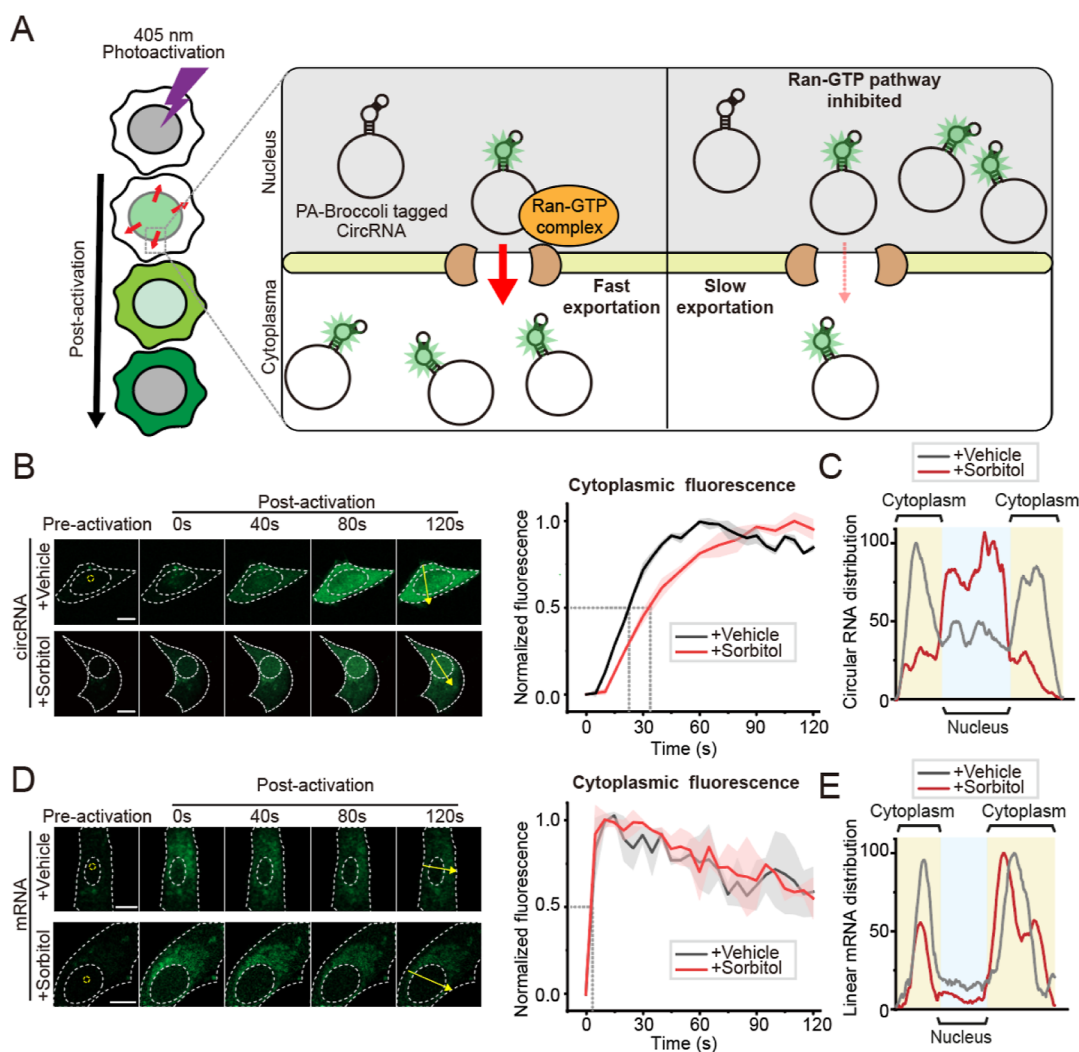
Figure 3. Distinct nuclear export mechanisms of circRNAs and mRNAs revealed by live subcellular imaging of PA-Broccoli. (A) Schematic of circRNA nuclear export dynamics monitored by PA-Broccoli in living cells. PA-Broccoli enables real-time visualization of circRNA nuclear export through nuclear pores (brown) via Ran-GTP-dependent transport (orange) mechanisms. Following local nuclear irradiation of PA-Broccoli-fused circRNAs, cytoplasmic Broccoli fluorescence accumulation rates were quantified to determine export kinetics. (B) Ran-GTP inhibition slows circRNA nuclear export imaged by PA-Broccoli. U2OS cells expressing Tornado-generated circular Broccoli RNA showed rapid fluorescence enhancement in both the nucleus and cytoplasm after local irradiation (405 nm laser, yellow circles) in the presence of PA3-BI (10 μM). The cytoplasmic Broccoli fluorescence of vehicle (DMSO)-treated cells increased rapidly with a $t_{1/2}$ of ~22 s (right). In contrast, the cytoplasmic fluorescence of sorbitol-treated cells showed a slower increase following nuclear light activation, with a $t_{1/2}$ of ~32 s (right). This indicates that sorbitol effectively inhibits the nuclear export of circular RNA. Data represent $n = 10$ cells from three independent experiments. Scale bar, 10 μm. The yellow arrow runs through the cell to produce the plot-profile in (C) (C) Inhibition of Ran-GTP leads to nuclear retention in circRNAs. Fluorescence intensity was quantified along the yellow line shown in (B). The resulting line profile revealed higher nuclear PA-Broccoli fluorescence in sorbitol-treated cells (red line) compared to vehicle-treated cells (gray line), indicating that sorbitol treatment impairs nuclear export of circRNAs. Similar RNA distribution patterns were observed in five independent cells. (D) Sorbitol does not affect mRNA nuclear export. We expressed 24xBroccoli tagged mRNA in U2OS cells, and irradiated the indicated nuclear regions (yellow circles, 405 nm laser) in the presence or absence of sorbitol (400 mM). In both conditions, cells showed rapid fluorescence enhancement in the nucleus and cytoplasm, with mRNA export kinetics and nuclear retention levels remaining unaffected by sorbitol treatment. This is in stark contrast to the behavior of circular RNA, where sorbitol treatment significantly impacts nuclear export. Quantification revealed that cytoplasmic Broccoli fluorescence of both vehicle and sorbitol-treated cells increased comparably, with a $t_{1/2}$ of ~3.7 s and no significant difference between groups ($p > 0.05$) (right). These results confirm that sorbitol specifically inhibits circRNA but not mRNA nuclear export. Data represent $n = 10$ cells from three independent experiments. Scale bar, 10 μm. The yellow arrow runs through the cell to produce the plot-profile in (E). (E) mRNA distribution is Ran-GTP-independent. Fluorescence intensity was quantified along the yellow lines shown in (D). Line profiles showed comparable nuclear and cytoplasmic fluorescence distributions in sorbitol-treated (red line) and vehicle-treated (gray line) cells, indicating that mRNA localization is not affected by Ran-GTP inhibition. Similar RNA-distribution patterns were observed in 5 independent cells.

We next sought to photolabel small noncoding RNA (ncRNA) tagged with PA-Broccoli tag in living cells. Certain small ncRNAs have specific subcellular localizations, for example, U6 RNA is localized in Cajal bodies.[38] We thus expressed the Broccoli-tagged U6 RNA in cells (Figure S11).

To localize Cajal bodies, we simultaneously coexpressed iRFP-fused SART3, a protein marker for Cajal bodies.[38] After local irradiation of the SART3-localized Cajal bodies, we observed enhanced green fluorescence colocalized with SART3-iRFP, indicating that the PA-Broccoli-tagged U6 RNA in the Cajal
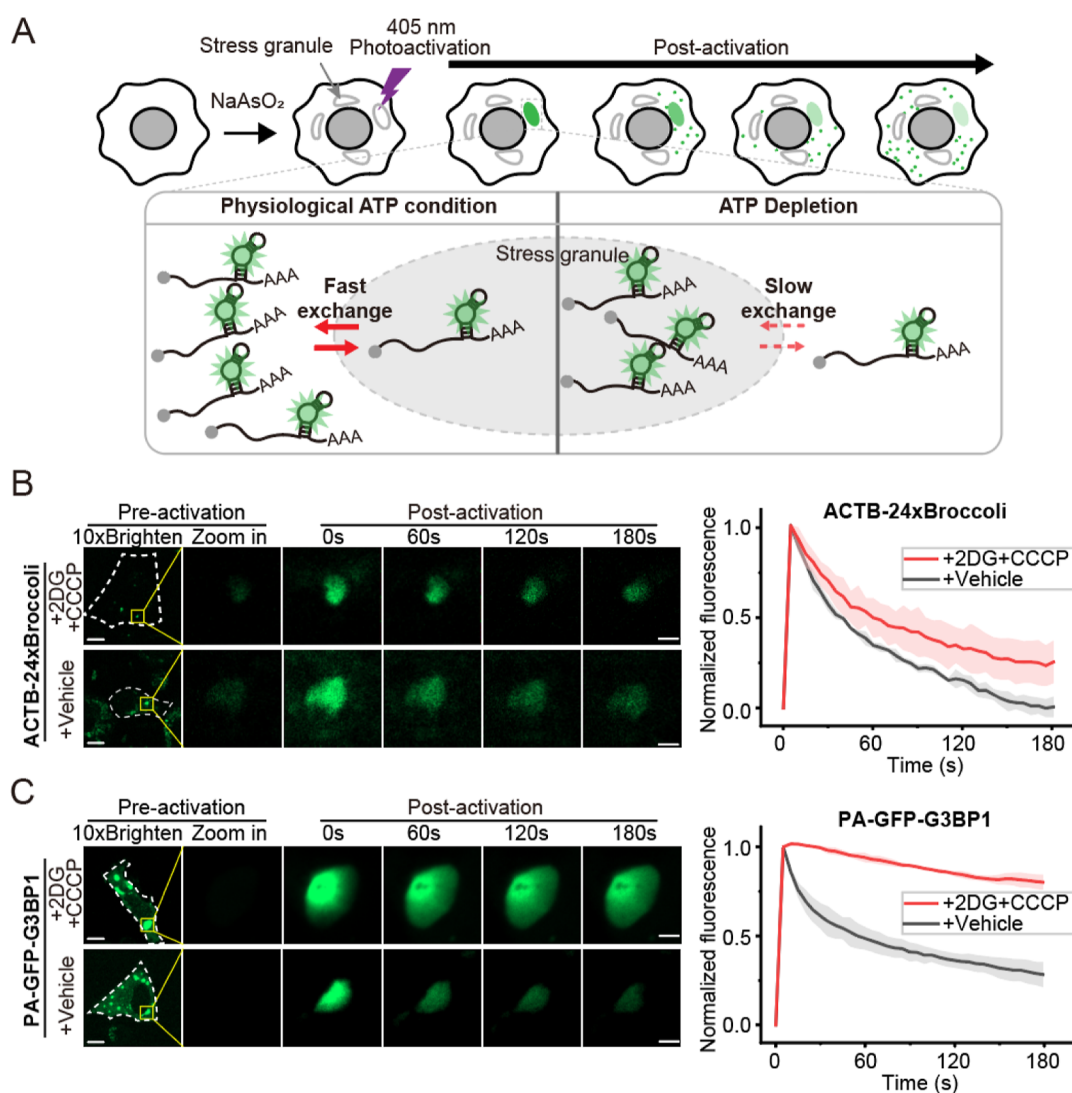
Figure 4. mRNA in stress granule exhibits energy-dependent exchange dynamics. (A) Schematic for monitoring ATP-dependent mRNA exchange dynamics in stress granules using PA-Broccoli. (B) Stress granule mRNA exportation is dependent on ATP. *ACTB*-Broccoli expressing U2OS cells were treated with NaAsO$_2$ (500 μM, 1 h) to induce stress granules, followed by ATP depletion (2DG + CCCP, 30 min, upper left). A single granule was photoactivated (405 nm laser, 5 W/cm^2, 2 μm spot) and imaged (Ex = 488 nm, Em = 525 $\pm$ 25 nm) for 180 s at 5 s intervals. Control cells without ATP depletion showed Broccoli fluorescence decay ($t_{1/2} \approx 26$ s, right), while ATP-depleted cells exhibited slower decay ($t_{1/2} \approx 60$ s, right). These results indicate that ATP depletion reduces the mRNA export rate from stress granules. Data represent $n = 10$ cells from three independent experiments. Scale bar, 10 μm (left), 2 μm (inset). (C) ATP-dependent G3BP1 export from stress granules imaged by PA-GFP. U2OS cells expressing PA-GFP-G3BP1 were treated as in (B). Photoactivated PA-GFP-G3BP1 in control cells treated with vehicle decayed rapidly ($t_{1/2} \approx 52$ s, right), while ATP-depleted cells treated with 2DG and CCCP showed slow decay ($t_{1/2} > 180$ s, right). These results suggest that in addition to mRNA, ATP depletion also reduces G3BP1 export rate.[51] Data represent $n = 10$ cells from three independent experiments. Scale bar, 10 μm (left), 2 μm (inset).

bodies was photoactivated (Figure S11). These results suggest that we can photolabel the specific ncRNAs at the subcellular level using PA-Broccoli.

We next spatiotemporally photoactivated subcellular DNA loci with PA-Broccoli. Previous work has shown that fluorogenic RNAs can be fused with small guide RNAs (sgRNA), which can then bind to deactivated Cas9 nuclease (dCas9), and be used to image chromosome loci in living cells.[39−41] To selectively label the gene of interest, we designed Broccoli-tagged sgRNA targeting a repetitive region of endogenous chromosome 3 (Chr3q29) (Figure S12A). Following the coexpression of the Broccoli-tagged sgRNA and dCas9-mCherry in U2OS cells, we localized three distinct loci of chromosome 3 trisomy, consistent with previous reports

of chromosomal aneuploidy in U2OS cells.[40−42] We then performed local irradiations sequentially, with each irradiation targeting a different locus. After each irradiation, we imaged the entire cell to monitor the activation of PA-Broccoli fluorescence (Figure S12B). We observed that the three green fluorescent puncta were sequentially photoactivated. This selective activation allows precise tracking of a specific genomic locus without interference from its homologous alleles.[40−45] Together, these data indicate that PA-Broccoli system allows sequential tracking of individual genomic loci.

Visualization of RNA Nuclear Export Dynamics via PA-Broccoli. To demonstrate the wide application of PA-Broccoli, we explored its use in visualizing circular RNA (circRNA) nuclear export. CircRNA biosynthesis begins with

transcription in the nucleus to produce linear RNAprecursors, and then circularization through intramolecular ligation mediated by ribozymes or back-splicing.[28,46] Since this RNA circularization process occurs exclusively in the nucleus, the resulting mature circRNAs must be exported from the nucleus to the cytoplasm.[46,47] Recent studies identified the key molecular components involved in circRNA export, including the Ran-GTP complex, which operates independently of mRNA export.[48] However, real-time kinetics and spatiotemporal regulation of circRNA export remain poorly understood.

To dynamically image circRNA nuclear exportation, we expressed circular Broccoli RNA[28] in PA3-BI-treated live U2OS cells (Figure 3A). Then, we locally irradiated the indicated regions in the nucleus with a 405 nm laser in the presence or absence of sorbitol-a known inhibitor of natural circRNA nuclear export due to its reduction of nuclear Ran levels.[48] By monitoring subsequent Broccoli fluorescence increase in the cytoplasm after irradiation, we were able to evaluate the efficiency and dynamics of circRNA export (Figure 3A). Our observations revealed that sorbitol-treated cells exhibited delayed cytoplasmic fluorescence accumulation, requiring ~32 s to reach half-maximal intensity ($t_{1/2}$). In contrast, untreated control cells exhibited a $t_{1/2}$ of ~22 s (Figure 3B). Moreover, we found that circRNA signal primarily localized to the nucleus in sorbitol-treated cells, whereas untreated cells showed stronger fluorescence in the cytoplasm (Figure 3C). These results indicate that Ran-GTP inhibition caused nuclear retention of circular RNA.

We also measured the Broccoli-tagged mRNA exportation in living cells in the presence or absence of sorbitol. In contrast to circRNA, mRNA exportation dynamics and distribution are not affected by sorbitol, with a $t_{1/2}$ of ~3.7 s (Figure 3D,E). Additionally, cells expressing Broccoli-tagged mRNA exhibited faster cytoplasmic fluorescence growth compared to circRNA-expressing cells, indicating that mRNA may have a faster exportation rate from the nucleus.[48-50] These findings highlight the differential export kinetics between circRNA and mRNA, and underscore the efficacy of PA-Broccoli in dissecting RNA export mechanisms in live cells.

mRNA Exchange Throughout Stress Granules is Energy-Dependent. We next sought to investigate RNA exchange dynamics across stress granules. Stress granules (SGs) are membrane-less cytoplasmic mRNA-protein (RNP) granules composed of translationally stalled mRNAs in response to various stresses[51] or diseases, including chemical stress, viral infections, cancer, and neurodegeneration.[51-54] The movement of mRNA entry and export from stress granules during stress regulates mRNA translation, mRNA storage and stabilization, and cell signaling.[51,53,55] Rapid mRNA exchange may prevent the complete stall of essential protein translation, while slow mRNA exchange could protect mRNA from degradation during prolonged stress.[51,52] Therefore, understanding the dynamics of mRNA exchange within stress granules, and how these dynamics are regulated, is crucial for elucidating how cells manage mRNA under stress conditions.

Since stress granule assembly includes the involvement of ATP-dependent RNA helicase,[51,52] we reasoned that the RNA exchange in stress granules could be ATP-dependent. To test this, we treated the cells expressing 24xBroccoli-tagged *ACTB* mRNA with sodium arsenite ($NaAsO_2$) for 1 h to induce stress granule formation (Figure 4A). Then, we incubated the cells with glycolysis inhibitor 2-deoxyglucose (2DG) and the oxidative phosphorylation uncoupler carbonyl cyanide *m*-chlorophenyl hydrazone (CCCP) to deplete intracellular ATP. We next locally irradiated G3BP1-localized stress granules and continuously recorded fluorescence in the irradiated regions (Figure 4A). In the absence of 2DG and CCCP, photoactivated granules displayed a rapid decay of Broccoli fluorescence intensity, with a median $t_{1/2}$ of ~26 s. On the contrary, ATP-depleted cells exhibited slower Broccoli fluorescence decay in photoactivated granules with a $t_{1/2}$ of ~60 s (Figure 4B). Since ATP depletion does not affect the diffusion dynamics of the photoactivated BI fluorophore alone within the stress granule (Figure S13A,B), the observed slower fluorescence decay in ATP-depleted cells likely reflects reduced exchange rates of RNA exit dynamics. This suggests that ATP plays a role in regulating the exchange of mRNA within stress granules, potentially through the activity of ATP-dependent RNA helicases.[52,56,57]

We also investigated the dynamics of PA-GFP-tagged G3BP1 protein under ATP depletion. Previous reports show that proteins in stress granules undergo reversible, continuous ATP-dependent movement from the stress granule.[51] To examine this, we locally irradiated a single stress granule in cells treated with or without 2DG and CCCP. As expected, PA-GFP-tagged G3BP1 diffused rapidly into the cytoplasm in untreated live U2OS cells, whereas G3BP1 was retained in the stress granule following ATP depletion (Figure 4C). Together, these results, combined with the observed changes in mRNA dynamics, suggest that ATP depletion affects both RNA and protein dynamics within stress granules, likely reducing their export rates.

■ CONCLUSION

Here, we developed an approach to design and optimize photoactivatable RNA tags for subcellular RNA imaging. Upon UV irradiation, these nonfluorescent tags were rapidly photoactivated, becoming highly fluorescent and enabling precise spatiotemporal labeling of subcellular RNA in living mammalian cells. Among these tags, PA-Broccoli demonstrates superior photoactivation characteristics compared to other photoactivatable RNA tags. Notably, PA-Broccoli achieves a remarkable ~6000-fold fluorescence enhancement with a rapid activation rate, exhibiting a $t_{1/2}$ of ~3 s. In contrast, its protein counterpart PA-GFP only shows a modest ~15-fold fluorescence increase and exhibits a $t_{1/2}$ of ~40 s. This high activation speed and fluorescence enhancement make PA-Broccoli ideal for tracking the subcellular RNA localization, movement, and interactions of RNA molecules in live cells.

Using PA-Broccoli, we visualized that cytoplasmic RNAs diffuse more slowly and show more restricted movement compared to proteins. This limited mobility may result from interactions with RNA-binding proteins, anchoring to cytoskeletal structures, or retention within organelle-associated compartments. These constraints suggest that cells actively regulate RNA positioning to control where and when RNAs are translated or degraded. By enabling direct localized photoactivation in living cells, PA-Broccoli provides a sensitive and precise tool for investigating RNA behavior.

Additionally, we employed PA-Broccoli to dynamically visualize circular RNA exportation from the nucleus. We found that circular RNA undergoes an export pathway that is different from linear mRNAs, with significantly slower kinetics. The export rate may indicate the functional fate of circRNAs: those designed for protein translation must efficiently reach the

cytoplasm, while regulatory circRNAs may need to be retained in the nucleus to perform gene silencing or transcriptional control. Our observations provide direct spatiotemporal evidence for differential transport behavior between linear and circular RNAs.

Moreover, we tracked mRNA dynamics through stress granules with PA-Broccoli, revealing the ATP dependency of mRNA export. Stress granules play a crucial role in regulating RNA fate during cellular stress. Previous studies showed that ATP is essential for protein dynamics within stress granules.[51] Our findings extend this to RNA, demonstrating that ATP is required for efficient mRNA export. Under physiological ATP conditions, mRNA in stress granules exhibits rapid exchange, which may facilitate translation reinitiation once stress subsides. In contrast, ATP depletion slows mRNA export, potentially stabilizing transcripts within stress granules to protect them from degradation during prolonged stress.[55,58]

In addition to Broccoli:BI system, the photoactivated approach can be extended to other fluorogenic RNA systems.[30,59−61] Using this strategy, we constructed a PA-RhoBAST system, which could also be photoactivated by UV irradiation but showed limited fluorescence enhancement compared to PA-Broccoli. This reduced performance may result from the electronic effects of the carboxyl group on TMR-DN, which could stabilize the photocaged structure and slow its dissociation.[26] Nevertheless, the general photo-activated approach remains applicable to other fluorogenic RNA systems.[39,62,63] For example, Nie lab developed a photoactivated Squash RNA system for cell-specific RNA labeling in live cells.[60] This flexibility in design allows for the development of orthogonal activation methods, enabling the tracking of different RNA populations in distinct subcellular compartments.

Furthermore, we developed NIR-activated PA-Broccoli by installing a Cy-NN caging group onto BI. However, compared to UV-activated PA-Broccoli, NIR-activated PA-Broccoli exhibited a lower activation fold and required prolonged exposure (Figure S7). These limitations are likely because of the lower photon energy of NIR light, which makes it more difficult to photoactivate Cy-NN-caged BI.[64] Despite the modest performance of NIR-activated PA-Broccoli, our results provide proof-of-concept for NIR-activated fluorescent RNA and highlight its potential for in vivo applications in the future.

In summary, photoactivatable fluorescent RNA, exemplified by PA-Broccoli, represents a transformative breakthrough in studying RNA dynamics across organelles and membranes. By enabling precise spatiotemporal control over RNA labeling, photoactivatable fluorescent RNA allows for dynamic tracking of RNA movements and detailed observation of their localization changes during cellular processes such as RNA transport and stress response. This approach bridges the gap between RNA real-time localization dynamics and its function, offering a powerful tool to dissect the molecular intricacies of RNA biology. Beyond fundamental research, the approach shows promising clinical potential for applications ranging from tumor-specific RNA visualization to surgical guid-ance.[65−69] These advancements deepen our understanding of RNA biology and hold significant potential for uncovering mechanisms, underlying cellular homeostasis, stress adaptation, and disease pathogenesis, and may also enable future clinical diagnostics and therapeutic strategies.

■ ASSOCIATED CONTENT

ⓢ Supporting Information

The Supporting Information is available free of charge at https://pubs.acs.org/doi/10.1021/jacs.5c07380.

Experimental section, HPLC results, bacteria imaging and other characterization of photoactivatable fluores-cent RNA (PDF)

■ AUTHOR INFORMATION

Corresponding Authors

Jinyang Zhang − *Interdisciplinary Science Center, State Key Laboratory of Animal Biodiversity Conservation and Integrated Pest Management, Institute of Zoology, Chinese Academy of Sciences, Beijing 100101, China; College of Life Sciences, University of Chinese Academy of Sciences, Beijing 100049, China;* Email: zhangjinyang@ioz.ac.cn

Pingyong Xu − *College of Life Sciences, University of Chinese Academy of Sciences, Beijing 100049, China; Key Laboratory of Biomacromolecules (CAS), CAS Center for Excellence in Biomacromolecules, Institute of Biophysics, Chinese Academy of Sciences, Beijing 100101, China;* ⓞ orcid.org/0000-0002-8779-6931; Email: pyxu@ibp.ac.cn

Xing Li − *Interdisciplinary Science Center, State Key Laboratory of Animal Biodiversity Conservation and Integrated Pest Management, Institute of Zoology, Chinese Academy of Sciences, Beijing 100101, China; Department of Pulmonary and Critical Care Medicine, The Affiliated Hospital of Southwest Medical University, Luzhou, Sichuan 646000, China; College of Life Sciences, University of Chinese Academy of Sciences, Beijing 100049, China;* ⓞ orcid.org/0000-0003-3149-9783; Email: li@ioz.ac.cn

Authors

Zhenyin Chen − *Interdisciplinary Science Center, State Key Laboratory of Animal Biodiversity Conservation and Integrated Pest Management, Institute of Zoology, Chinese Academy of Sciences, Beijing 100101, China; Department of Pulmonary and Critical Care Medicine, The Affiliated Hospital of Southwest Medical University, Luzhou, Sichuan 646000, China; College of Life Sciences, University of Chinese Academy of Sciences, Beijing 100049, China; Hangzhou Institute of Medicine, Chinese Academy of Sciences, Hangzhou 310018 Zhejiang, China*

Haodong Jiang − *Interdisciplinary Science Center, State Key Laboratory of Animal Biodiversity Conservation and Integrated Pest Management, Institute of Zoology, Chinese Academy of Sciences, Beijing 100101, China; College of Life Sciences, University of Chinese Academy of Sciences, Beijing 100049, China*

Lin Yuan − *Key Laboratory of Biomacromolecules (CAS), CAS Center for Excellence in Biomacromolecules, Institute of Biophysics, Chinese Academy of Sciences, Beijing 100101, China*

Tuoxin Yao − *College of Life Sciences, Hunan Normal University, Changsha 410081, China*

Xiaoxiao Rong − *Interdisciplinary Science Center, State Key Laboratory of Animal Biodiversity Conservation and Integrated Pest Management, Institute of Zoology, Chinese Academy of Sciences, Beijing 100101, China; College of Life Sciences, University of Chinese Academy of Sciences, Beijing 100049, China*

Wankai Gao − *Interdisciplinary Science Center, State Key Laboratory of Animal Biodiversity Conservation and Integrated Pest Management, Institute of Zoology, Chinese Academy of Sciences, Beijing 100101, China; College of Life Sciences, University of Chinese Academy of Sciences, Beijing 100049, China*

Chenhang Zeng − *College of Life Sciences, Hebei University, Baoding, Hebei 071002, China*

Liuqin He − *College of Life Sciences, Hunan Normal University, Changsha 410081, China*

Yulong Yin − *Yuelushan Laboratory, Changsha 410128, China; Institute of Subtropical Agriculture, Chinese Academy of Sciences, Changsha 410125, China*

Samie R. Jaffrey − *Department of Pharmacology, Weill Cornell Medicine, Cornell University, New York, New York 10065, United States;* ⊙ orcid.org/0000-0003-3615-6958

Fangqing Zhao − *Interdisciplinary Science Center, State Key Laboratory of Animal Biodiversity Conservation and Integrated Pest Management, Institute of Zoology, Chinese Academy of Sciences, Beijing 100101, China; College of Life Sciences, University of Chinese Academy of Sciences, Beijing 100049, China*

Complete contact information is available at:
https://pubs.acs.org/10.1021/jacs.5c07380

Author Contributions

◆Zhenyin Chen and Haodong Jiang contributed equally.

Notes

The authors declare no competing financial interest.

■ REFERENCES

(1) Chalfie, M.; Tu, Y.; Euskirchen, G.; Ward, W. W.; Prasher, D. C. Green Fluorescent Protein as a Marker for Gene Expression. *Science* **1994**, *263* (5148), 802−805.

(2) Patterson, G. H.; Lippincott-Schwartz, J. A photoactivatable GFP for selective photolabeling of proteins and cells. *Science* **2002**, *297* (5588), 1873−1877.

(3) Lukyanov, K. A.; Chudakov, D. M.; Lukyanov, S.; Verkhusha, V. V. Innovation: Photoactivatable fluorescent proteins. *Nat. Rev. Mol. Cell Biol.* **2005**, *6* (11), 885−891.

(4) Chudakov, D. M.; Matz, M. V.; Lukyanov, S.; Lukyanov, K. A. Fluorescent proteins and their applications in imaging living cells and tissues. *Physiol. Rev.* **2010**, *90* (3), 1103−1163.

(5) Testa, I.; Parazzoli, D.; Barozzi, S.; Garre, M.; Faretta, M.; Diaspro, A. Spatial control of pa-GFP photoactivation in living cells. *J. Microsc.* **2008**, *230* (1), 48−60.

(6) Chudakov, D. M.; Belousov, V. V.; Zaraisky, A. G.; Novoselov, V. V.; Staroverov, D. B.; Zorov, D. B.; Lukyanov, S.; Lukyanov, K. A. Kindling fluorescent proteins for precise in vivo photolabeling. *Nat. Biotechnol.* **2003**, *21* (2), 191−194.

(7) Tulu, U. S.; Rusan, N. M.; Wadsworth, P. Peripheral, non-centrosome-associated microtubules contribute to spindle formation in centrosome-containing cells. *Curr. Biol.* **2003**, *13* (21), 1894−1899.

(8) Chudakov, D. M.; Verkhusha, V. V.; Staroverov, D. B.; Souslova, E. A.; Lukyanov, S.; Lukyanov, K. A. Photoswitchable cyan fluorescent protein for protein tracking. *Nat. Biotechnol.* **2004**, *22* (11), 1435−1439.

(9) Lee, W. L.; Kim, M. K.; Schreiber, A. D.; Grinstein, S. Role of ubiquitin and proteasomes in phagosome maturation. *Mol. Biol. Cell* **2005**, *16* (4), 2077−2090.

(10) Subach, F. V.; Patterson, G. H.; Renz, M.; Lippincott-Schwartz, J.; Verkhusha, V. V. Bright monomeric photoactivatable red fluorescent protein for two-color super-resolution sptPALM of live cells. *J. Am. Chem. Soc.* **2010**, *132* (18), 6481−6491.

(11) Paige, J. S.; Wu, K. Y.; Jaffrey, S. R. RNA mimics of green fluorescent protein. *Science* **2011**, *333* (6042), 642−646.

(12) Li, X.; Mo, L.; Litke, J. L.; Dey, S. K.; Suter, S. R.; Jaffrey, S. R. Imaging Intracellular S-Adenosyl Methionine Dynamics in Live Mammalian Cells with a Genetically Encoded Red Fluorescent RNA-Based Sensor. *J. Am. Chem. Soc.* **2020**, *142* (33), 14117−14124.

(13) Chen, W.; Zhao, X.; Yang, N.; Li, X. Single mRNA Imaging with Fluorogenic RNA Aptamers and Small-molecule Fluorophores. *Angew. Chem., Int. Ed.* **2023**, *62* (7), No. e202209813.

(14) Chen, Z.; Chen, W.; Reheman, Z.; Jiang, H.; Wu, J.; Li, X. Genetically encoded RNA-based sensors with Pepper fluorogenic aptamer. *Nucleic Acids Res.* **2023**, *51* (16), 8322−8336.

(15) Li, X.; Kim, H.; Litke, J. L.; Wu, J.; Jaffrey, S. R. Fluorophore-Promoted RNA Folding and Photostability Enables Imaging of Single Broccoli-Tagged mRNAs in Live Mammalian Cells. *Angew. Chem., Int. Ed.* **2020**, *59* (11), 4511−4518.

(16) Filonov, G. S.; Moon, J. D.; Svensen, N.; Jaffrey, S. R. Broccoli: rapid selection of an RNA mimic of green fluorescent protein by fluorescence-based selection and directed evolution. *J. Am. Chem. Soc.* **2014**, *136* (46), 16299−16308.

(17) Song, W.; Strack, R. L.; Svensen, N.; Jaffrey, S. R. Plug-and-play fluorophores extend the spectral properties of Spinach. *J. Am. Chem. Soc.* **2014**, *136* (4), 1198−1201.

(18) Li, X.; Wu, J.; Jaffrey, S. R. Engineering Fluorophore Recycling in a Fluorogenic RNA Aptamer. *Angew. Chem., Int. Ed.* **2021**, *60* (45), 24153−24161.

(19) Wu, J.; Zaccara, S.; Khuperkar, D.; Kim, H.; Tanenbaum, M. E.; Jaffrey, S. R. Live imaging of mRNA using RNA-stabilized fluorogenic proteins. *Nat. Methods* **2019**, *16* (9), 862−865.

(20) Gan, Q.; Xu, G.; Deng, X.; Liu, M.; Deng, Y.; Lu, W.; Ruan, Y.; Fu, C.; Yu, Y. Self-assembly solid-state enhanced fluorescence emission of GFP chromophore analogues: Formation of microsheets and microtubes oriented by molecular skeleton. *J. Colloid Interface Sci.* **2024**, *654* (Pt A), 698−708.

(21) Luo, J.; Xie, Z.; Lam, J. W.; Cheng, L.; Chen, H.; Qiu, C.; Kwok, H. S.; Zhan, X.; Liu, Y.; Zhu, D.; et al. Aggregation-induced emission of 1-methyl-1,2,3,4,5-pentaphenylsilole. *Chem. Commun.* **2001**, *18*, 1740−1741.

(22) Warner, K. D.; Chen, M. C.; Song, W.; Strack, R. L.; Thorn, A.; Jaffrey, S. R.; Ferre-D'Amare, A. R. Structural basis for activity of highly efficient RNA mimics of green fluorescent protein. *Nat. Struct. Mol. Biol.* **2014**, *21* (8), 658−663.

(23) Barltrop, J. A.; Plant, P. J.; Schofield, P. Photosensitive protective groups. *Chem. Commun.* **1966**, No. 22, 822−823.

(24) Patchornik, A.; Amit, B.; Woodward, R. B. Photosensitive protecting groups. *J. Am. Chem. Soc.* **1970**, *92* (21), 6333−6335.

(25) Cummings, R. T.; Krafft, G. A. Photoactivable fluorophores. 1. Synthesis and photoactivation ofo-nitrobenzyl-quenched fluorescent carbamates. *Tetrahedron Lett.* **1988**, *29* (1), 65−68.

(26) Bochet, C. G.; Blanc, A. Photolabile Protecting Groups in Organic Synthesis. In *Handbook of Synthetic Photochemistry*; Wiley, 2009; pp 417−447.

(27) Paige, J. S.; Nguyen-Duc, T.; Song, W.; Jaffrey, S. R. Fluorescence imaging of cellular metabolites with RNA. *Science* **2012**, *335* (6073), 1194.

(28) Litke, J. L.; Jaffrey, S. R. Highly efficient expression of circular RNA aptamers in cells using autocatalytic transcripts. *Nat. Biotechnol.* **2019**, *37* (6), 667−675.

(29) Henderson, J. N.; Gepshtein, R.; Heenan, J. R.; Kallio, K.; Huppert, D.; Remington, S. J. Structure and mechanism of the photoactivatable green fluorescent protein. *J. Am. Chem. Soc.* **2009**, *131* (12), 4176−4177.

(30) Sunbul, M.; Lackner, J.; Martin, A.; Englert, D.; Hacene, B.; Grun, F.; Nienhaus, K.; Nienhaus, G. U.; Jaschke, A. Super-resolution RNA imaging using a rhodamine-binding aptamer with fast exchange kinetics. *Nat. Biotechnol.* **2021**, *39* (6), 686−690.

(31) Zhang, Y.; Xu, Z.; Xiao, Y.; Jiang, H.; Zuo, X.; Li, X.; Fang, X. Structural mechanisms for binding and activation of a contact-quenched fluorophore by RhoBAST. *Nat. Commun.* **2024**, *15* (1), 4206.

(32) Song, H.; Reheman, Z.; Fang, Y.; Jiang, H.; Hou, R.; Shi, Y.; Weng, Y.; Li, X.; Liu, L. RNA-Based Fluorescent Sensor with RhoBAST. *Anal. Chem.* **2025**.

(33) Gorka, A. P.; Nani, R. R.; Zhu, J.; Mackem, S.; Schnermann, M. J. A near-IR uncaging strategy based on cyanine photochemistry. *J. Am. Chem. Soc.* **2014**, *136* (40), 14153−14159.

(34) Braga, J.; McNally, J. G.; Carmo-Fonseca, M. A reaction-diffusion model to study RNA motion by quantitative fluorescence recovery after photobleaching. *Biophys. J.* **2007**, *92* (8), 2694−2703.

(35) Keskin, O.; Jernigan, R. L.; Bahar, I. Proteins with similar architecture exhibit similar large-scale dynamic behavior. *Biophys. J.* **2000**, *78* (4), 2093−2106.

(36) Eisen, T. J.; Eichhorn, S. W.; Subtelny, A. O.; Lin, K. S.; McGeary, S. E.; Gupta, S.; Bartel, D. P. The Dynamics of Cytoplasmic mRNA Metabolism. *Mol. Cell* **2020**, *77* (4), 786−799.e10.

(37) Lampo, T. J.; Stylianidou, S.; Backlund, M. P.; Wiggins, P. A.; Spakowitz, A. J. Cytoplasmic RNA-Protein Particles Exhibit Non-Gaussian Subdiffusive Behavior. *Biophys. J.* **2017**, *112* (3), 532−542.

(38) Novotny, I.; Malinova, A.; Stejskalova, E.; Mateju, D.; Klimesova, K.; Roithova, A.; Sveda, M.; Knejzlik, Z.; Stanek, D. SART3-Dependent Accumulation of Incomplete Spliceosomal snRNPs in Cajal Bodies. *Cell Rep.* **2015**, *10* (3), 429−440.

(39) Chen, X.; Zhang, D.; Su, N.; Bao, B.; Xie, X.; Zuo, F.; Yang, L.; Wang, H.; Jiang, L.; Lin, Q.; et al. Visualizing RNA dynamics in live cells with bright and stable fluorescent RNAs. *Nat. Biotechnol.* **2019**, *37* (11), 1287−1293.

(40) Ma, H.; Tu, L. C.; Naseri, A.; Huisman, M.; Zhang, S.; Grunwald, D.; Pederson, T. Multiplexed labeling of genomic loci with dCas9 and engineered sgRNAs using CRISPRainbow. *Nat. Biotechnol.* **2016**, *34* (5), 528−530.

(41) Zhang, Z.; Rong, X.; Xie, T.; Li, Z.; Song, H.; Zhen, S.; Wang, H.; Wu, J.; Jaffrey, S. R.; Li, X. Fluorogenic CRISPR for genomic DNA imaging. *Nat. Commun.* **2024**, *15* (1), 934.

(42) Ma, H.; Tu, L. C.; Naseri, A.; Chung, Y. C.; Grunwald, D.; Zhang, S.; Pederson, T. CRISPR-Sirius: RNA scaffolds for signal amplification in genome imaging. *Nat. Methods* **2018**, *15* (11), 928−931.

(43) Chen, B.; Gilbert, L. A.; Cimini, B. A.; Schnitzbauer, J.; Zhang, W.; Li, G. W.; Park, J.; Blackburn, E. H.; Weissman, J. S.; Qi, L. S.; et al. Dynamic imaging of genomic loci in living human cells by an optimized CRISPR/Cas system. *Cell* **2013**, *155* (7), 1479−1491.

(44) Qin, P.; Parlak, M.; Kuscu, C.; Bandaria, J.; Mir, M.; Szlachta, K.; Singh, R.; Darzacq, X.; Yildiz, A.; Adli, M. Live cell imaging of low- and non-repetitive chromosome loci using CRISPR-Cas9. *Nat. Commun.* **2017**, *8* (1), 14725.

(45) Wang, H.; Nakamura, M.; Abbott, T. R.; Zhao, D.; Luo, K.; Yu, C.; Nguyen, C. M.; Lo, A.; Daley, T. P.; La Russa, M.; et al. CRISPR-mediated live imaging of genome editing and transcription. *Science* **2019**, *365* (6459), 1301−1305.

(46) Liu, C. X.; Chen, L. L. Circular RNAs: Characterization, cellular roles, and applications. *Cell* **2022**, *185* (12), 2016−2034.

(47) Kim, J. Circular RNAs: Novel Players in Cancer Mechanisms and Therapeutic Strategies. *Int. J. Mol. Sci.* **2024**, *25* (18), 10121.

(48) Ngo, L. H.; Bert, A. G.; Dredge, B. K.; Williams, T.; Murphy, V.; Li, W.; Hamilton, W. B.; Carey, K. T.; Toubia, J.; Pillman, K. A.; et al. Nuclear export of circular RNA. *Nature* **2024**, *627* (8002), 212−220.

(49) Grunwald, D.; Singer, R. H.; Rout, M. Nuclear export dynamics of RNA-protein complexes. *Nature* **2011**, *475* (7356), 333−341.

(50) Li, Z.; Kearse, M. G.; Huang, C. The nuclear export of circular RNAs is primarily defined by their length. *RNA Biol.* **2019**, *16* (1), 1−4.

(51) Jain, S.; Wheeler, J. R.; Walters, R. W.; Agrawal, A.; Barsic, A.; Parker, R. ATPase-Modulated Stress Granules Contain a Diverse Proteome and Substructure. *Cell* **2016**, *164* (3), 487−498.

(52) Chalupnikova, K.; Lattmann, S.; Selak, N.; Iwamoto, F.; Fujiki, Y.; Nagamine, Y. Recruitment of the RNA helicase RHAU to stress granules via a unique RNA-binding domain. *J. Biol. Chem.* **2008**, *283* (50), 35186−35198.

(53) Marcelo, A.; Koppenol, R.; de Almeida, L. P.; Matos, C. A.; Nobrega, C. Stress granules, RNA-binding proteins and polyglutamine diseases: too much aggregation? *Cell Death Dis.* **2021**, *12* (6), 592.

(54) Xu, Q.; Ma, Y.; Sun, Y.; Li, D.; Zhang, X.; Liu, C. Protein amyloid aggregate: Structure and function. *Aggregate* **2023**, *4* (4), No. e333.

(55) Moon, S. L.; Morisaki, T.; Khong, A.; Lyon, K.; Parker, R.; Stasevich, T. J. Multicolour single-molecule tracking of mRNA interactions with RNP granules. *Nat. Cell Biol.* **2019**, *21* (2), 162−168.

(56) Chen, M. C.; Tippana, R.; Demeshkina, N. A.; Murat, P.; Balasubramanian, S.; Myong, S.; Ferre-D'Amare, A. R. Structural basis of G-quadruplex unfolding by the DEAH/RHA helicase DHX36. *Nature* **2018**, *558* (7710), 465−469.

(57) Lu, Z.; Xu, J.; Chen, Y.; Zhou, Y.; Zhou, X.; Wang, Q.; Wei, Q.; Han, S.; Zhao, R.; Weng, X.; et al. Rapid degradation of DHX36 revealing its transcriptional role by interacting with G-quadruplex. *Aggregate* **2025**, *6* (1), No. e647.

(58) Chen, Z.; Duan, H.; Li, X. In vivo single-molecule RNA structural profiling. *Trends Biochem. Sci.* **2023**, *48* (3), 211−212.

(59) Englert, D.; Burger, E. M.; Grun, F.; Verma, M. S.; Lackner, J.; Lampe, M.; Buhler, B.; Schokolowski, J.; Nienhaus, G. U.; Jaschke, A.; et al. Fast-exchanging spirocyclic rhodamine probes for aptamer-based super-resolution RNA imaging. *Nat. Commun.* **2023**, *14* (1), 3879.

(60) Yin, P.; Huang, C.; Zhang, L.; Li, Z.; Zhong, C.; Kuang, S.; Lei, C.; Huang, Y.; Nie, Z. Developing Orthogonal Fluorescent RNAs for Photoactive Dual-color Imaging of RNAs in Live Cells. *Angew. Chem., Int. Ed.* **2025**, *64*, No. e202424060.

(61) Qiao, Q.; Liu, W.; Chi, W.; Chen, J.; Zhou, W.; Xu, N.; Li, J.; Fang, X.; Tao, Y.; Zhang, Y.; et al. Modulation of dynamic aggregation in fluorogenic SNAP-tag probes for long-term super-resolution imaging. *Aggregate* **2023**, *4* (2), No. e258.

(62) Dey, S. K.; Filonov, G. S.; Olarerin-George, A. O.; Jackson, B. T.; Finley, L. W. S.; Jaffrey, S. R. Repurposing an adenine riboswitch into a fluorogenic imaging and sensing tag. *Nat. Chem. Biol.* **2022**, *18* (2), 180−190.

(63) Truong, L.; Kooshapur, H.; Dey, S. K.; Li, X.; Tjandra, N.; Jaffrey, S. R.; Ferre-D'Amare, A. R. The fluorescent aptamer Squash extensively repurposes the adenine riboswitch fold. *Nat. Chem. Biol.* **2022**, *18* (2), 191−198.

(64) Klan, P.; Solomek, T.; Bochet, C. G.; Blanc, A.; Givens, R.; Rubina, M.; Popik, V.; Kostikov, A.; Wirz, J. Photoremovable protecting groups in chemistry and biology: reaction mechanisms and efficacy. *Chem. Rev.* **2013**, *113* (1), 119−191.

(65) Dong, H.; Lei, J.; Ding, L.; Wen, Y.; Ju, H.; Zhang, X. MicroRNA: function, detection, and bioanalysis. *Chem. Rev.* **2013**, *113* (8), 6207−6233.

(66) Kitto, R. Z.; Christiansen, K. E.; Hammond, M. C. RNA-based fluorescent biosensors for live cell detection of bacterial sRNA. *Biopolymers* **2021**, *112* (1), No. e23394.

(67) Zhang, Y. P.; Wang, Z. G.; Tian, Y. F.; Jiang, L. H.; Zhao, L.; Kong, D. M.; Li, X.; Pang, D. W.; Liu, S. L. In Situ Self-Assembly of Fluorogenic RNA Nanozipper Enables Real-Time Imaging of Single

Viral mRNA Translation. *Angew. Chem., Int. Ed.* **2023**, *62* (25), No. e202217230.

(68) Chen, Z.; Chen, W.; Xu, C.; Song, H.; Ji, X.; Jiang, H.; Duan, H.; Li, Z.; Gao, W.; Yao, T.; et al. Near-infrared fluorogenic RNA for in vivo imaging and sensing. *Nat. Commun.* **2025**, *16* (1), 518.

(69) Sun, J.; Li, H.; Gu, X.; Tang, B. Z. Photoactivatable Biomedical Materials Based on Luminogens with Aggregation-Induced Emission (AIE) Characteristics. *Adv. Healthcare Mater.* **2021**, *10* (24), No. e2101177.